Journal of Colloid and Interface Science 450 (2015) 316–324

Contents lists available at ScienceDirect

Journal of Colloid and Interface Science

www.elsevier.com/locate/jcis

Regular Article

Simple thiol-ene click chemistry modification of SBA-15 silica pores with carboxylic acids

Andrea V. Bordoni [a,*], M. Verónica Lombardo [a], Alberto E. Regazzoni [a], Galo J.A.A. Soler-Illia [a,b], Alejandro Wolosiuk [a,*]

[a] Gerencia Química – Centro Atómico Constituyentes, Comisión Nacional de Energía Atómica, Av. Gral. Paz 1499 B1650KNA San Martín, Buenos Aires, Argentina
[b] DQIAyQF, FCEN, Universidad de Buenos Aires, Ciudad Universitaria, Pabellón II, C1428EHA Buenos Aires, Argentina

GRAPHICAL ABSTRACT

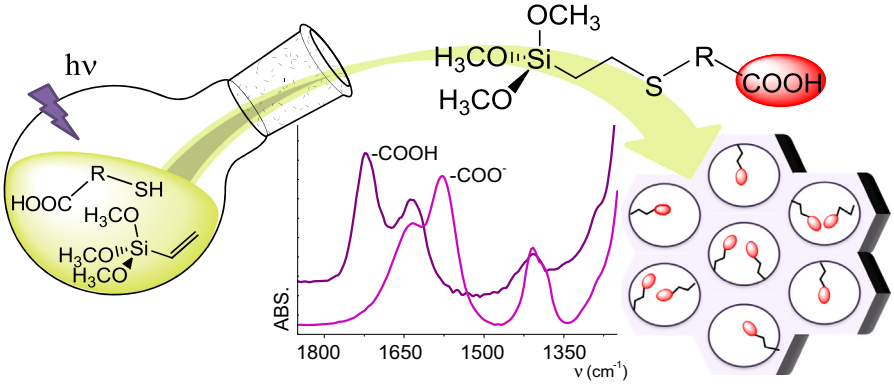

ARTICLE INFO

Article history:
Received 31 December 2014
Accepted 13 March 2015
Available online 21 March 2015

Keywords:
Mesostructured materials
Functionalized SiO_2
Carboxylic groups
Click chemistry
Thiol-ene addition
SBA-15

ABSTRACT

A straightforward approach for anchoring tailored carboxylic groups in mesoporous SiO_2 colloidal materials is presented. The thiol-ene photochemical reaction between vinyltrimethoxysilane precursors and various thiocarboxylic acids which has, click chemistry features (i.e. high conversion yields, insensitivity to oxygen, mild reaction conditions), results in carboxylated silane precursors that can be readily used as surface modifiers. The carboxylic groups of acetic, undecanoic and succinic acid were immobilized on the silica mesopore walls of SBA-15 powders employing the synthesized silane precursors. Post-grafting has been confirmed through infrared spectrometry (FTIR), energy dispersive X-ray spectroscopy (EDS), elemental analysis (EA) and zeta potential measurements. Detailed field-emission gun scanning electron microscopy (FESEM) images and small angle X-ray scattering (SAXS) data revealed parallel mesopores and ordered mesostructures. It is shown that the immobilized COOH groups are chemically accessible for acid–base reactions as well as copper adsorption. Immobilization of easily synthesized tailored carboxylic modified alkoxide precursors within mesoporous systems provides a unique chemical nanoenvironment within these ordered frameworks.

1. Introduction

SiO_2 mesoporous materials (MM) with uniform pore size (2–50 nm) and high surface areas (600–1500 m^2/g) stand as highly functional platforms that can fulfill multiple purposes: protein

Abbreviations: PG, post grafting; MSA, mercaptosuccinic acid; MUDA, mercaptoundecanoic acid; MAA, mercaptoacetic acid; TEOS, Tetraethylorthosilicate; EtOAc, ethylacetate.

* Corresponding authors.
E-mail addresses: bordonia@gmail.com (A.V. Bordoni), wolosiuk@cnea.gov.ar (A. Wolosiuk).

http://dx.doi.org/10.1016/j.jcis.2015.03.030
0021-9797/

immobilization, sensing, adsorption and drug delivery [1–4]. The enhanced surface/mass ratio of these materials opens an exciting perspective for tailoring the pore surface chemistry for specific purposes. The functionalization of the pore wall surface of MM with organosilanes imparts new chemical properties that can be directed to various applications: polymer brushes for "gated" controlled release of ions [5,6], enzyme responsive systems [7], controlled epoxidation catalysis [8] and noble metals adsorption [9] while pore size determines its sieving properties [10–12]. Within this context, the chemistry of carboxylic groups is of extreme importance because it has both scientific and technologic implications: provides pH dependent surface charges for adsorption and catalytic processes [13,14], modulates the adhesion of biocompatible surfaces and their immunogenic reaction [15], is an important ligand for metallic cations [16], serves as a nanoparticle stabilizer [17] and anchoring sites for protein immobilization [18]. Unfortunately, the commercial availability of carboxylic group derivatized alkoxides is scarce and carboxyethylsilanetriol ($(OH)_3Si(CH_2)_2COONa$) stands as one of the very few options for COOH silica modification [19–21]. This molecule has already been used for cisplatin drug delivery [22] and for the synthesis of SBA-15 mesoporous materials featuring zwitterionic surfaces [23,24]. As pointed out in a recent review [24], the anchoring of carboxylic groups on SiO_2 materials has been solved, albeit partially following diverse strategies: hydrolysis of 2-cyanoethyltriethoxysilane in concentrated H_2SO_4 and high temperature [25,26], condensation of maleic anhydride and 3-mercaptopropylsilane in a Michael addition reaction [27], or hydrosilylation of protected carboxyl groups [28,29]. Nonetheless, it is desirable to find a general approach that would allow the control of the length of the methylene chain or the number of carboxylic end groups as these factors define the interfacial and electronic charge transfer properties of the solid/solution boundary [30].

The construction of a versatile library of precursors containing carboxylic moieties needs a simple but effective coupling chemistry. In this sense, *click chemistry* is becoming the "weapon of choice" for both precursor synthesis and surface modification [31–33]. Azide based chemistry is one of the most popular click reactions since Sharpless et al. developed the concept in 2001 [34]. The cooper-catalyzed azide-alkyne cycloaddition (CuAAC) reaction is a powerful tool for covalently binding two organic molecules resulting in a 1,4-disubstituted-1,2,3-triazole linker, and has been used on polymers, surfaces and nanoparticles [35]. This reaction protocol has the following advantages: excellent yields, extensive commercial availability of azide and alkyne derivatized molecules and synthetic orthogonality. On the downside, CuAAC requires the use of O_2-free environments and Cu(I) as catalyst, which can be disadvantageous for biological samples as well as for surface properties. Furthermore, it involves the handling of explosive azides.

The radical-initiated thiol-ene reaction is known since the beginning of 20th century and has been widely used in polymer synthesis due to the homogeneity of the networks produced [36,37]. Recently, this reaction scheme has found increasing utility along multiple areas (e.g. materials science, surface chemical modification, dendrimer synthesis) as it has proven to have "click characteristics" [34,38]. In fact, the high chemoselectivity and mild reaction conditions make it orthogonal [39] with most organic functional groups (—COOH, —NH_2, —CH_2OH). Moreover, there is no need of O_2-free or anhydrous conditions. In addition, the abundant commercial availability of thiol and vinyl based molecules and the possibility to initiate the reaction photochemically make it highly attractive for tailored patterned surface modification [40]. Recently, Tucker-Schwartz et al. exploited the characteristics of the radical thiol-ene chemistry, and reported the synthesis of a wide library of tailored modified alkoxysilanes between mercaptopropylsilane and allyl or terminal alkenes based on radical thiol-ene chemistry [41].

Here, we make use of this working scheme to react thiocarboxylic acids with vinyltrimethoxysilane in order to obtain free functionalized carboxyl derivatized silanes, and illustrate the easiness of the SBA-15 pore surface modification with these precursors. The immobilization of the COOH groups was confirmed by FTIR, zeta potential, EA and EDS measurements.

FE-SEM, N_2 sorption and SAXS showed that the post-grafted COOH modified silanes conserve the mesostructure of the original SBA-15 powders. Furthermore, it is shown that the immobilized carboxylic groups are readily available for copper adsorption.

2. Materials and methods

2.1. Materials

Tetraethylorthosilicate (98%, TEOS), vinyltrimethoxysilane (98%, VTMS), mercaptoacetic acid (97%, MAA), mercaptoundecanoic acid (95%, MUDA), 2-mercaptosuccinic acid (97%, MSA), benzophenone (99%, Ph_2CO) and Pluronic® P123 were purchased from Sigma–Aldrich and used as received. Hydrochloric acid 37%, methanol, ethanol, chloroform, toluene, n-heptane and ethylacetate (EtOAc) were purchased from Merck. Methanol, ethanol, chloroform and toluene were dried over activated MS-3 Å before use.

2.2. Synthesis

2.2.1. Synthesis and characterization of silane carboxylic precursors for SBA-15 surface modification

2-((2-(Trimethoxysilyl)ethyl)thio)succinic acid (TMSMSA), 2-((2-(trimethoxysilyl)ethyl)thio) acetic acid (TMSMAA) and 2-((2-(trimethoxysilyl)ethyl)thio)undecanoic acid (TMSMUDA) were prepared by the thiol-ene click reaction. Typically, VTMS was added to a solution containing the desired thioacid and Ph_2CO to reach a final composition of 1:1:0.2 mole ratio; in the cases of MAA and MSA, the solvent of choice was methanol, whereas chloroform was used to solubilize MUDA. Reaction solutions were then irradiated, under gentle stirring, for 16 h using a 15 W, 18″-long black-light lamp (λ_{max} = 352 nm).

The times required to attain reaction completion were assessed by thin layer chromatography (TLC) using 0.2 mm silica gel 60 F254 aluminum-supported plates (Merck); detection was effected by exposure to UV light followed by immersion in $KMnO_4$ stain. In all cases, the analyses showed that VTMS disappears in less than 16 h (Rf 0.75; n-heptane-EtOAc 6:4).

Reaction products were characterized by NMR, using a Bruker AM 500 spectrometer at 500 MHz (^1H) and 125.8 MHz (^{13}C); the residual peak of $CDCl_3$ was used as internal reference. Assignments were supported by ^1H-COSY and HSQC experiments.

2.2.2. Synthesis of SBA-15

SBA-15 was prepared following the method reported by Zhao et al. [42] Briefly, 4 g Pluronic® P123 was dissolved in a 1.6 M HCl aqueous solution (150 g), and 8.5 g TEOS was added. The solution was then kept at 35 °C for 20 h under constant stirring. Afterwards, the resulting colloidal dispersion was left undisturbed at 90 °C for 24 h. The solid product was recovered by filtration, washed with water and ethanol, and dried overnight at 60 °C. Finally, the solid was calcined at 500 °C for 6 h; the temperature ramp was 1 °C min^{-1}.

2.2.3. Surface modification of SBA-15

Carboxylic functional groups were anchored to the surface of SBA-15 by post-grafting. For this purpose, 1.1 g SBA-15 was dispersed in 150 ml dry toluene, and the appropriate volume of the

crude, unpurified, click-reaction product containing 4.5 mmol TMSMSA, TMSMAA or TMSMUDA was added. The suspension was then left standing under stirring for 24 h, at room temperature. The product was filtered, washed with toluene and ethanol, and dried at room temperature for 24 h in vacuum.

Solids modified with TMSMSA, TMSMAA and TMSMUDA shall hereafter be labelled as SBA–MSA, SBA–MAA and SBA–MUDA, respectively.

2.3. Characterization of SBA-15 and surface modified SBA-15

2.3.1. N_2 adsorption/desorption

Nitrogen adsorption–desorption isotherms at 77 K were measured in a Micromeritics ASAP 2420 equipment. Surface area was calculated by using the BET equation. The total pore volume was obtained at $P/P_0 = 0.95$, and the micropore volume was calculated from the *t*-Plot. Pore size was obtained from the desorption branch using the BJH (Barrett–Joyner–Halenda) model.

2.3.2. Zeta potential measurements

Samples were prepared by adding different amounts of HCl or KOH to diluted SBA-15 and modified SBA-15 aqueous suspensions; ionic strength was fixed at 10 mM using KCl. The measurements were performed in a Zetasizer 2000 (Malvern Instruments Ltd.) while pH values were measured using a pH-meter HI 3222 (Hanna Instruments). All suspensions were equilibrated at least 2 h in order to obtain stable pH and zeta potential readings.

2.3.3. SEM images

Field emission scanning electron microscopy (FESEM) images and energy dispersive spectroscopy (EDS) spectra were taken with a ZEISS LEO 982 GEMINI field emission electron microscope in the secondary electron mode, using an in-lens detector to improve resolution. Samples for imaging were prepared by dispersing the mesoporous SiO_2 powders on a Si wafer. EDS measurements were performed in at least 4 different spots; samples were exclusively deposited onto a carbon tape.

2.3.4. FTIR measurements

Infrared Fourier transform spectroscopy measurements were performed with a Nicolet Magna 560 instrument, equipped with liquid N_2 cooled MCT-A detector in transmission mode. Samples, as well as the KBr used for pellet preparation, were dried under vacuum overnight.

2.3.5. Powder SAXS measurements

SAXS measurements were performed at SAXS1 beamline of the Brazilian Synchrotron Light Laboratory (LNLS) under remote operation mode. SBA-15 solid powders were placed in a multiple position sample holder. The scattered beam ($\lambda = 1.55$ Å) was detected in a Pilatus 300k (Dectris AG, Switzerland) detector placed 884 mm away from the sample holder.

2.3.6. Elemental analysis

Atomic C, N and S composition were determined using an Exeter CE 440 Chemical Analyzer with a thermal conductivity detector.

2.3.7. Carboxylic conversion to carboxylate

To observe the availability of the carboxylic groups present in the modified porous particles, the samples were first exposed to a 0.1 M HCl solution for 10 min. Then, the supernatant was withdrawn by centrifugation, and the solid contacted with 0.01 M NaOH for 10 min. Finally, the solid samples were separated, dried and inspected by FTIR.

2.3.8. Copper adsorption

10 mg of the synthesized powders (SBA-15 and SBA–MSA) were suspended in 10 ml of $CuSO_4$ aqueous solutions of varying concentrations (10–300 ppm), and stirred at room temperature for 6 h. Afterwards, solids were recovered by centrifugation, and the copper content of the supernatant solutions was analyzed by the sodium diethyldithiocarbamate (DDTC) method [43].

Preliminary kinetic experiments demonstrated that adsorption attains constant values in less than 15 min; for the sake of simplicity, however, equilibration times were set at 6 h.

3. Results and discussion

3.1. Synthesis of carboxyl functionalized alkoxysilanes

As mentioned in the Introduction, immobilization of carboxylic functional groups on SiO_2 surfaces lacks the commercial availability of silanes with COOH moieties. Thus, appropriate precursors ought to be synthesized beforehand. In the present approach, the synthesis of the carboxyltrialkoxysilanes derivatives resorts to the easy and simple photochemically initiated thiol-ene addition reaction. Equally important, the obtained precursors do not require purification prior their use as surface modifiers.

Fig. 1a shows the ^{1}H NMR of the crude reaction mixture of MAA with VTMS according to Scheme 1 (TMSMUDA and TMSMSA NMR spectra are provided as Supplementary Material). In agreement with the observed disappearance of VTMS by TLC, the ^{1}H NMR spectra of the crude reaction of TMSMSA, TMSMUDA and TMSMAA show the absence of the typical deshielded resonance of vinyl protons at large δ ($\delta \sim 6.5$–5.8 ppm) from VTMS [44]. Moreover, the ^{1}H NMR spectra denote the appearance of a signal at high fields ($\delta \sim 0.9$ ppm) due to the protons of the methylene group bonded to Si [45] after thioether bond formation. These two facts strongly support the successful synthesis of the derivatized carboxysilanes as there are no other ^{1}H signals in this region related to the reactants.

The previous results have been also confirmed by ^{13}C NMR on the same crude reaction mixture as shown in Fig. 1b (see other ^{1}H NMR and ^{13}C NMR precursors in Supplementary Material). The presence of a signal at $\delta \sim 10$ ppm in the ^{13}C NMR spectra, assigned to the α-C (with respect to Si) in the derivatized silane, indicates the change in hybridization from the VTMS double bond (sp^2) to a single bond (sp^3) after addition of the thiocarboxylic acid. Again, there are no signals from any of the reactants in this region of the ^{13}C spectrum, confirming the formation of a thioether bond.

Clearly, these photoinitiated thiol-ene click reactions, which attain total reactant conversion after UV irradiation, involve extremely simple synthetic steps that do not require organic synthesis skills or specialized equipment. In contrast to CuAAC click reactions, the photochemical thiol-ene reaction does not require N_2 atmosphere, since it overcomes oxygen inhibition [40]. In summary, this method allows to obtain significant quantities of carboxylic based silanes for silica surface modification through an easy and affordable chemical approach that, as it will be shown below, does not require any purification step.

3.2. Synthesis and characterization of the mesoporous SiO_2 matrices

3.2.1. SAXS measurements and FE-SEM images

The controlled hydrolysis-condensation of silica precursors in acidic medium in the presence of Pluronics® P123 template results in a highly mesostructured material, whose surface can be easily COOH-functionalized via post-grafting using the crude reaction products of the thiol-ene addition reactions. Fig. 2 shows the SAXS patterns of the synthesized SBA-15 and of the surface modified SBA–MAA, SBA–MSA and SBA–MUDA materials. The analysis

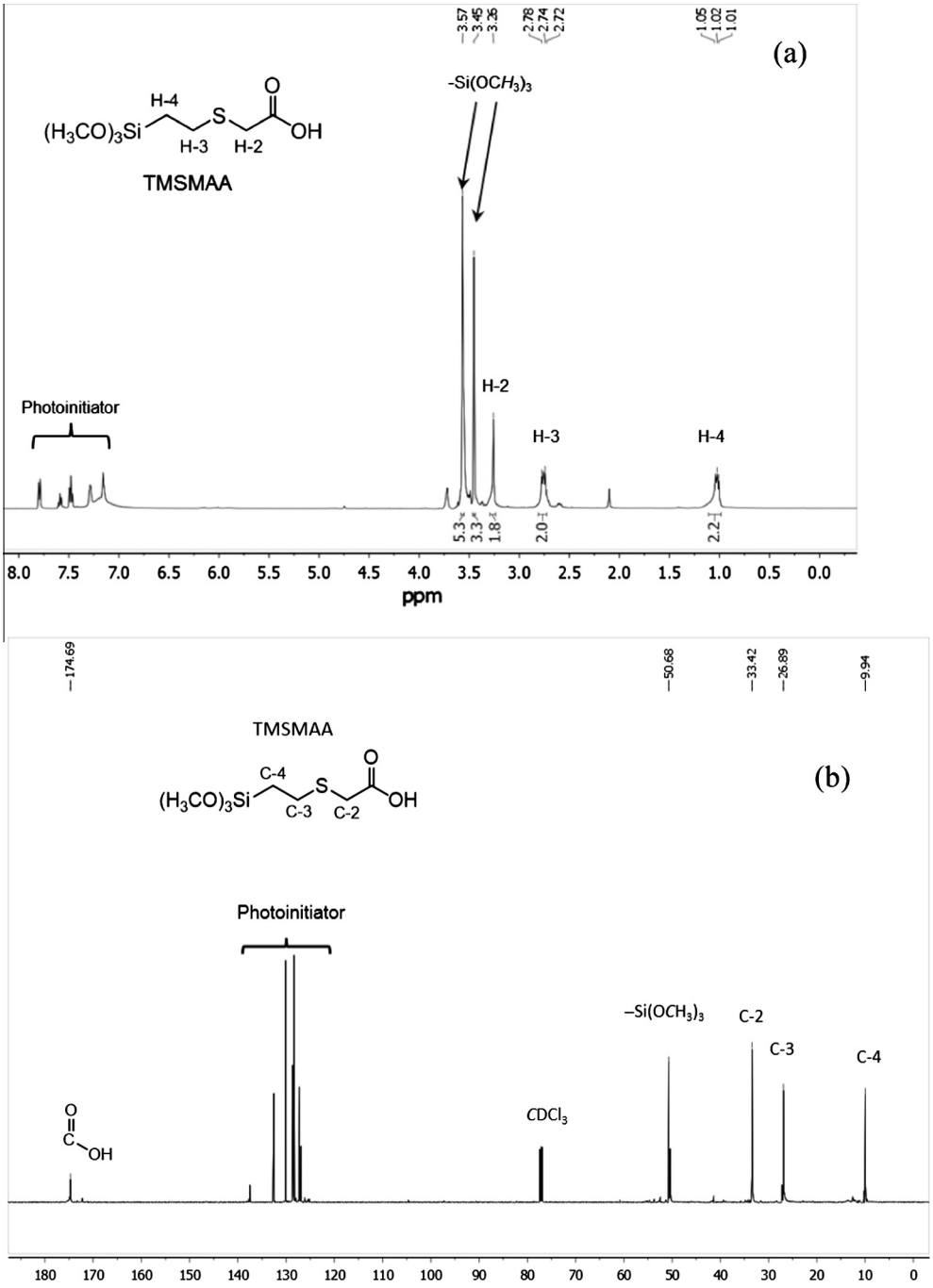

Fig. 1. (a) ^{1}H NMR (500 MHz, $CDCl_3$) and (b) ^{13}C NMR (128.5 MHz, $CDCl_3$) of TMSMAA crude reaction without purification.

of the peak distances points to a 2D hexagonal structure (space group *p6mm*), thus reflections were indexed according to Eq. (1), which corresponds to a general hexagonal symmetry, with the *l* parameter equated to zero (i.e., all peaks correspond to (*hk*0) planes); in Eq. (1), *d* is the interplanar spacing, and *a* is the cell parameter. In particular, for SBA-15 based materials, *d* represents the pore to pore distance in a 2D hexagonal symmetry.

$$\frac{1}{d^2} = \frac{4}{3}\left(\frac{h^2 + hk + k^2}{a^2}\right) + \frac{l^2}{c^2} \quad (1)$$

The so derived cell parameters are listed in Table 1. They are typical of SBA mesoporous materials. It is known that *a* and *d* depend not only on the synthesis conditions, but also on the conditions of the post-treatment [42,46–48]. Nonetheless, similarities of the observed cell parameters indicates that both the mesostructure and the 2D hexagonal order are preserved after the post-grafting functionalization of SBA-15 with the synthesized TMSMAA, TMSMSA and TMSMUDA precursors.

Fig. 2 also shows the appearance and the disappearance of certain reflections after the functionalization of the SBA-15 mesopores with the COOH derivatized silanes. This behavior can, in principle, be attributed to differences in the electronic contrast between the silica walls and the functional groups, preferential chemical modification of micropores, or subtle morphology changes in pore shape [49,50]. The full explanation of this phenomenon is however beyond the scope of this work.

The high order of the mesoporous structures is further revealed by the FE-SEM images presented in Fig. 3. Fig. 3a illustrates the

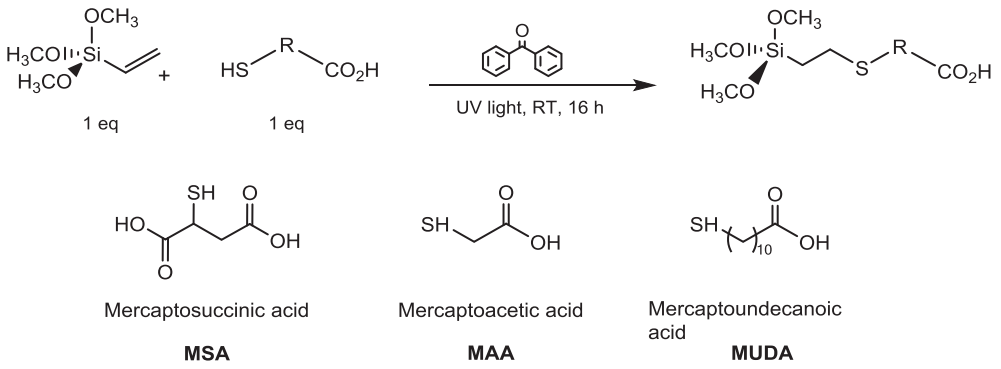

Scheme 1. Generalized click chemistry reaction scheme and modified thioacids.

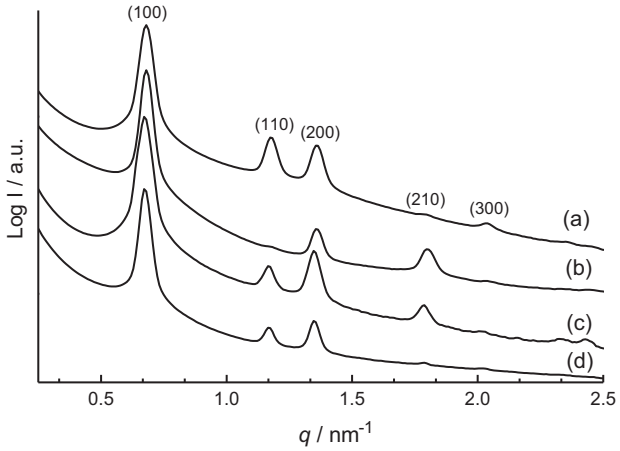

Fig. 2. SAXS for SBA-15 (a), SBA–MSA (b), SBA–MAA (c) and SBA–MUDA (d). The numbers in parentheses are the Miller indexes of the mesoporous structure.

morphology of the SBA-15 particles, which are elongated; their length being 800 ± 60 nm, and the width 500 ± 50 nm. At a higher magnification, the channel-like structures of their mesoporous array become evident (Fig. 3b–d); channels run parallel to the longer particle axis and form the typical 2D hexagonal porous arrange of SBA-15 materials [42]. Comparison of Fig. 3b–d further shows that SBA-15 particles modified by post-grafting with TMSMSA keeps the initial pore mesostructure, in line with SAXS results. Similar FE-SEM images have been obtained for SBA-MAA and SBA-MUDA modified powders (see Supplementary Material).

In summary, it can be concluded that post-functionalization of SBA-15 with the carboxylic derivatized silanes does not affect its mesoporous framework. Furthermore, these results show that the photoinitiator of the thiol-ene reaction, which is present in the crude product used for functionalization (Fig. 1), has no effect.

3.2.2. N_2 porosimetry

The nitrogen adsorption/desorption isotherms obtained at 77 K for SBA-15 and functionalized SBA-15 mesoporous materials are presented in Fig. 4a, where type IV curves with H1 hysteresis loops along with sharp volume increases in the range $p/p_0 = 0.5–0.7$ are observed [51,52]. Both bare and modified SBA-15 materials show parallel adsorption/desorption branches suggesting cylindric monodispersed mesopores [53]. BET surface areas, total pore volumes (calculated by Gurvitch method), micropore volumes (calculated from *t*-Plots (Mesopore Volume = Total Pore Volume − Micropore Volume)) and pore diameters (calculated by the BJH method) are given in Table 2. It can be seen that, at first glance, the measured surface area of all the COOH derivatized SBA-15 powders are noticeably lower than that of pristine SBA-15 solids. This reduction in area should be expected as chemical functional groups are immobilized on the pore surface. Likewise, the pore diameter and the mesopore volume of the COOH modified SBA particles show a similar contraction. The pore size distributions remain narrow, as it is usual for post-grafting modifications [54]. In addition, the microporosity of all modified SBA-15 samples decreases substantially, which suggests that surface condensation of derivatized silanes may have taken place preferentially at the micropores surfaces, thus filling the micropore cavities. It is noteworthy, that both monocarboxylic acids, MAA and MUDA, show approximately the same reduction of pore diameter, while the MSA modified surface that bears about twice the amount of COOH functional groups exhibits a more marked diminution of pore size. Nonetheless, it has to be kept in mind that N_2, which has a quadrupolar moment, may present strong interactions with the COOH modified SiO_2 surface [55]; in fact, adsorption/desorption isotherms models used for pore characterization are based on non-interacting adsorbents.

Table 1
Cell parameters for SBA-15 and SBA-15 post grafted with carboxylic silanes: d represents the interplanar spacing and a, the cell parameter obtained by SAXS.

	d/nm	*a*/nm
SBA-15	9.2	10.7
SBA–MSA	9.2	10.7
SBA–MAA	9.4	10.8
SBA–MUDA	9.4	10.8

3.2.3. EA and EDS measurements

In order to assess the degree of COOH functionalization of the SBA-15 powders, we employed EA, for detecting the immobilized thioether's sulfur atoms. Table 3 presents the content of sulfur in the functionalized SBA-15, which are stoichiometrically related to the COOH loading in the SBA-15 powders. As expected from the synthesis conditions that were set, these figures vary slightly, their differences reflecting the molecular weight of the precursors used for surface modification. Sulfur to silicon mole ratios obtained by EDS are also given in Table 3. Comparison of these data is not straightforward. Nonetheless, on the basis of rather safe assumptions (i.e., all of the detected Si is expressed as SiO_2; the mass of the modified SBA materials is given by the sum of the masses of SiO_2 and the organic skeletons of the grafted functions), the EDS information is in qualitative agreement with EA data. The data in Table 3 demonstrate that the starting SBA-15 material has been successfully functionalized by the simple approach proposed here. However, they give no information about the degree of the SBA-15 surface that has been functionalized. Assuming that the number of

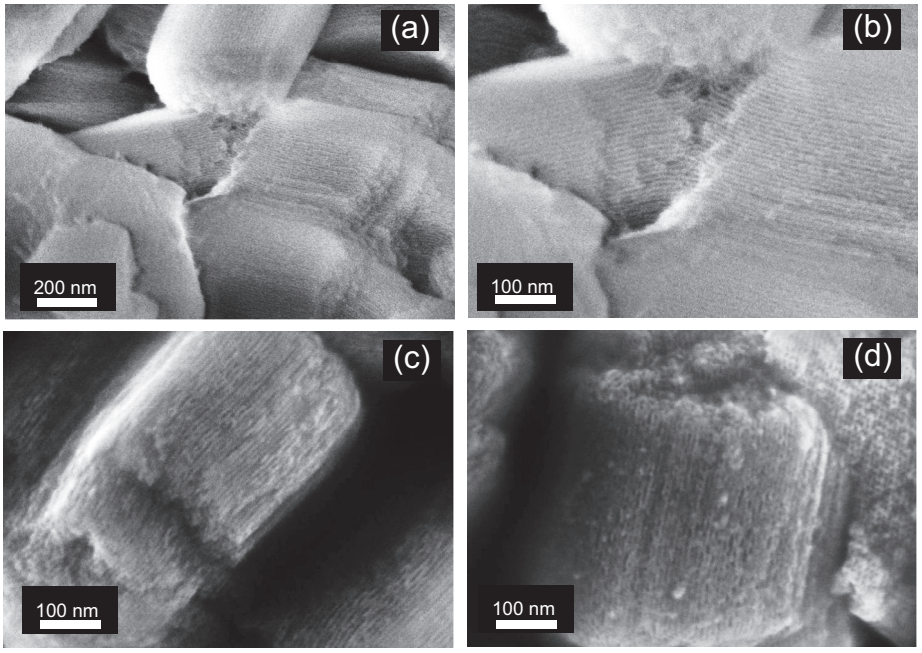

Fig. 3. (a and b) FE-SEM micrographs of unmodified SBA-15 particles; (c and d) SBA–MSA.

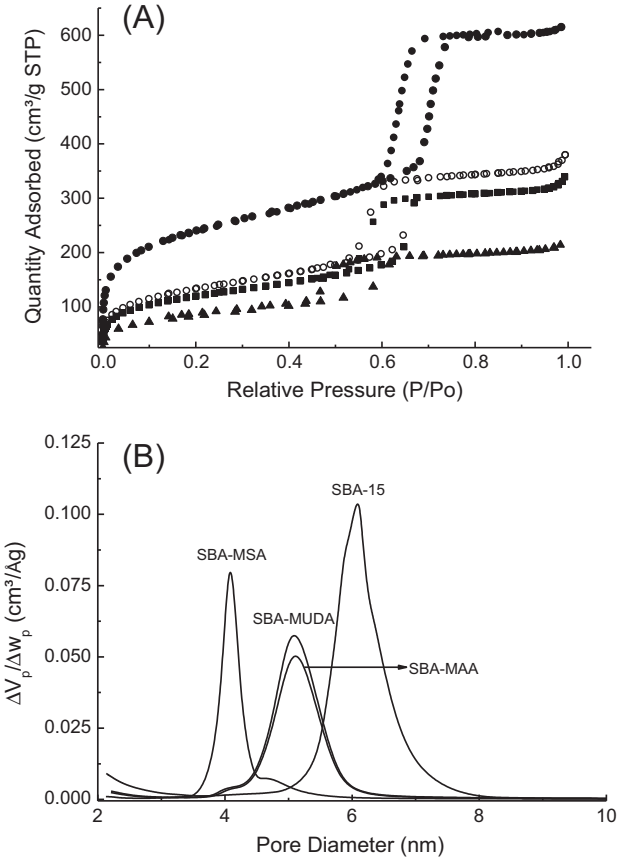

Fig. 4. (a) Nitrogen adsorption - desorption curves for SBA-15 (●), SBA–MUDA (○), SBA–MAA (■) and SBA–MSA (▲). (b) Pore size distributions for SBA-15 and SBA-15 COOH modified powders.

silanol surface groups of SBA-15 is close to 4.6 OH nm^{-2}, the Zhuralev constant [56], the amount of TMSMSA, TMSMAA and TMSMUDA used in the post-grafting step should suffice to form a monolayer, if the precursors attach to the SBA-15 surface through 3 SiOH; in fact, the used amount of precursor is in excess with respect to the estimated quantity of available SiOH sites. Assuming once again, that the mass of the modified materials is the mass of SBA-15 plus that of the grafted moieties, the amount of anchoring sites per gram of functionalized material can be estimated to be 4.7 mmol g^{-1}, which is 3.1 times larger than its sulfur content (1.5 mmol g^{-1}). These numbers suggest that a monolayer may actually have been form on the SBA-15 surface, despite the uncertainties of the above assumptions. The excess precursor remains either unreacted or hydrolyzes and self-condense to form toluene soluble species.

Below, we will analyze the accessibility of the immobilized COOH chemical groups.

3.2.4. FTIR measurements

Fig. 5 shows the FTIR spectra of SBA-15 of SBA-15 modified with TMSMSA, TMSMUDA and TMSMAA. All of them depict the typical C═O stretch located at 1722 cm^{-1}. This band is actually the result of the superposition of the C═O stretching modes of various possible carboxylic moieties (dimeric, oligomeric, isolated, etc.) that are present in the confined environments of the mesoporous frameworks; such moieties were recently identified in the detailed spectroscopic work of Gershevitz and Sukenik [57]. The band due to the C—O bend is present at 1406 cm^{-1}. Other possible bands due to the anchored functional groups in the 1200–800 cm^{-1} region are completely masked by the strong Si—O—Si vibrations.

In all cases, sorbed water is manifested by the broad band at 3600–3000 cm^{-1} that corresponds to the OH stretch of water molecules interacting through hydrogen bonding with surface silanol (SBA-15) and anchored carboxylic groups (SBA–MAA, SBA–MSA and SBA–MUDA). Also, the band at 1630 cm^{-1}, due to scissoring of the OH groups, is evident in all spectra, except that for SBA–MUDA. Clearly, SBA–MUDA shows the weakest water signal, despite all samples have been dried following the same procedure. This must reflect the higher hydrophobicity of SBA–MUDA that is bestowed by its long methylene chain. In fact, the antisymmetric and symmetric stretching modes of —CH_2, at 2920 and 2849 cm^{-1}, are only distinguishable in the case of SBA–MUDA. It is worth mentioning here that the hydrophobic nature of

Table 2
Surface area and pore features for SBA-15 and carboxylic-modified SBA samples.

	Surface area (m^2/g)	Total volume (cm^3/g)	Micropore volume (cm^3/g)	Mesopore volume (cm^3/g)	Pore diameter (nm)
SBA-15	874	0.94	0.17	0.77	6.1
SBA–MSA	301	0.32	0.03	0.29	4.3
SBA–MUDA	482	0.52	0.07	0.45	5.0
SBA–MAA	433	0.49	0.05	0.44	5.0

Table 3
Sulfur loading in the carboxylic-modified SBA-15 powders.

	Sulfur mmoles/g[a]	S/Si atomic ratio[b]	Sulfur mmoles/g[c]
SBA–MSA	1.5 ± 0.1	0.09 ± 0.01	1.2 ± 0.1
SBA–MAA	1.5 ± 0.1	0.11 ± 0.03	1.5 ± 0.3
SBA–MUDA	0.8 ± 0.1	0.09 ± 0.01	1.1 ± 0.1

[a] EA.
[b] EDS.
[c] Estimate from EDS measurements.

SBA–MUDA powders is also reflected by their colloidal behavior; particles float, initially, when suspended in water.

It can therefore be concluded that although all modified materials share the same COOH functional end group, the nanoenvironment of these mesoporous systems is markedly different, even for a simple molecule, such as water. In addition, these results show that the photoinitiator, which is present in the crude product of the thiol-ene reaction (Scheme 1), has no influence on the immobilization of the carboxylic groups.

3.2.5. Chemical accessibility of carboxylate groups and zeta potential measurements

The above results demonstrate that our simple synthesis approach allows the preparation of mesoporous SBA particles with COOH functionalized surfaces. However, they are silent as to whether these groups are accessible and prone to react with dissolved solutes. Recently, Fiorilli et al. have used titration with gaseous ammonia for probing the accessibility of the COOH groups generated after the hydrolysis of butyronitrile groups [58,59]. However, since our interest is to exploit the surface properties of the functionalized SBA materials in aqueous solutions, we turn our attention into their deprotonation/protonation behavior. For this purpose, we have contacted the solids with NaOH and HCl solutions, sequentially, and inspected them by FTIR after drying.

Fig. 6 shows that there is a simple and clear correlation between the $COOH/COO^-$ FTIR signals and the nature of swamping media.

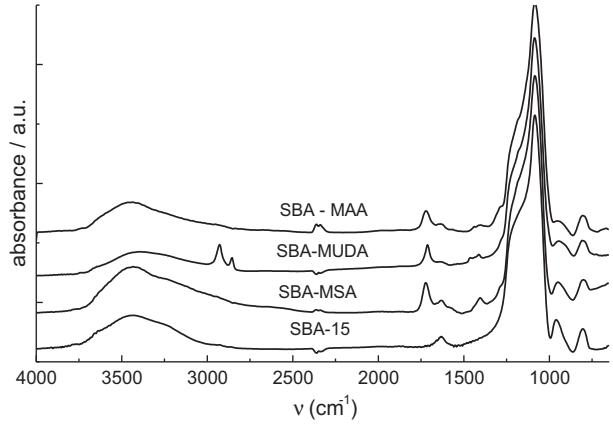

Fig. 5. FTIR spectra of SBA-15 and COOH modified SBA-15 powders in the 4000–800 cm^{-1} region.

The typical band due to the antisymmetrical stretching vibration of carboxylate, located at 1580–1565 cm^{-1}, develops upon deprotonation in alkaline solutions. Conversely, the band at 1722 cm^{-1} disappears. The opposite is seen when the deprotonated functionalized SBA materials are immersed in acidic solutions. As expected, the band at ca. 1400 cm^{-1} is much less sensitive towards pH changes.

It is interesting to note that the position of the $\nu_{a(COO-)}$ band shifts as the length of the methylene chain increases; for SBA–MAA, SBA–MSA and SBA–MUDA, this band appears at 1580, 1577 and 1565 cm^{-1}, respectively. This latter value compares very well with that attributed to carboxylate groups at air/solid interfaces [60], a fact that suggests that the anchored COO^- also experience the hydrophobic environment of the SBA–MUDA mesopores.

Summing up, these experiments show that the post-grafted COOH groups are available for simple acid–base reactions, and should be expected to engage in other chemical reactions.

Post-functionalization should modify not only the inner pores of SBA-15, but also its external surface. Zeta potential measurements (Table 4) show that, upon functionalization, the negative overall surface charge of the particles increases at any given pH. This is consistent with the deprotonation of the immobilized COOH groups; possible isolated Si—OH groups [61], also contribute to particle charging up. In addition, the observed trend correlates very well with the p*K*a values of MSA, MUDA and MAA (MSA: $pK_1 = 3.3$; $pK_2 = 4.9$ [62]; MUDA: $pK_1 = 4.9$; MAA: $pK_1 = 3.65$ [63]). In this context, the ζ-potential measurements support qualitatively the previous FTIR observations, demonstrating that the SBA-15 surfaces were successfully functionalized with pH responsive carboxylic groups.

3.2.6. Copper adsorption

In order to test the accessibility of carboxylic groups to ions other than hydroxide or protons, the capacity of SBA–MSA materials to adsorb copper was evaluated. Cu^{2+} is a common pollutant related to different industrial activities such as mining and electroplating [64] and has been used as a fungicide in the past [65]. It is a fact that carboxylate groups form metal coordination complexes with many divalent ions, such as Cu^{2+} [66], and by the same token, should form stable surface complexes. Fig. 7 shows adsorption isotherms for SBA-15 and SBA–MSA. As expected, the pristine SBA-15 surface has no appreciable affinity for Cu^{2+} at the explored conditions, whereas significant copper quantities are adsorbed by the SBA–MSA material. Moreover, the Cu^{2+} uptake rate is fast and reaches saturation in 30 min (see Supplementary Material). This behavior has as already been observed for amine and thiol modified SBA-15 powders [67].

The adsorption data were adjusted according to Equation (2), where q_e is the actual Cu^{2+} loading, C_e is the remnant equilibrium concentration, Q_0 is the maximum adsorption capacity, and b is a constant related to the intensity of adsorption.

$$q_e = \frac{Q_0 b C_e}{1 + bC_e} \quad (2)$$

This expression was linearized (see, Supplementary Material), and the value $Q_0 = 56 \pm 4$ mg g^{-1} was derived. Q_0 can also be expressed

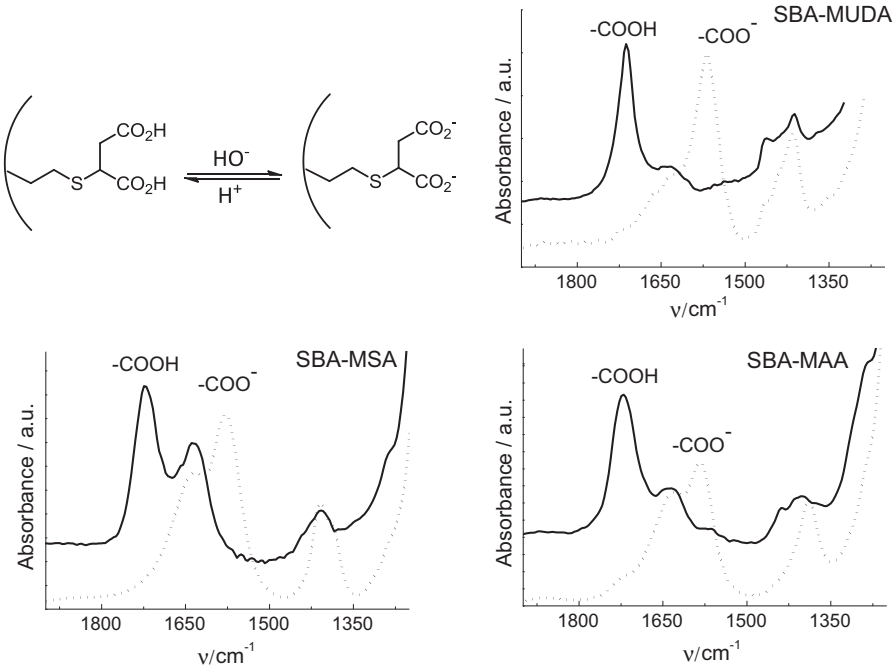

Fig. 6. FTIR spectra of COOH modified SBA-15 powders exposed to acidic and alkaline environments.

Table 4
Zeta potential of SBA-15 and COOH modified SBA-15 particles.

ζ-potential (mV)	pH 3	pH 5	pH 9
SBA-15	2.6	−7.1	−31.9
SBA−MSA	−23.3	−44.4	−44.0
SBA−MUDA	−14.5	−39.9	−36.8
SBA−MAA	−15.4	−39.2	−37.0

as 0.88 mmol Cu^{2+} g^{-1}, a value that is a third of the total amount of COOH groups (N_{COOH}) assessed by EA measurements (Table 3); note that the number of carboxylic groups in SBA–MSA is twice the amount of sulfur. Bearing in mind that adsorbed Cu^{2+} ions may bind to two or more anchored carboxylates, the observed Q_0/N_{COOH} ratio indicates that most of the immobilized carboxylic groups are available for complexation. Notwithstanding, the FTIR spectrum of an SBA–MSA sample loaded with 0.9 mmol Cu^{2+} g^{-1} (Fig. 8) denotes the presence of protonated groups, even at a condition that is saturation. Naturally, at equilibrium, a distribution of complexed and free carboxylic surface groups must exist. Fig. 8 also shows that

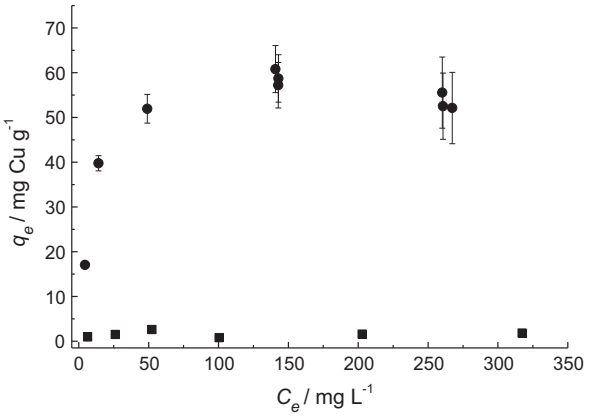

Fig. 7. Copper adsorption isotherms for: SBA-15 (■) and SBA–MSA (●).

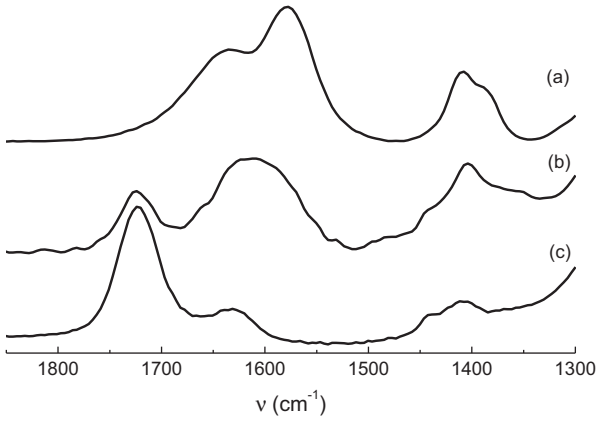

Fig. 8. FTIR spectra of SBA–MSA after HO^- treatment (a), 0.9 mmol Cu^{2+} g^{-1} adsorption (b) and H^+ treatment (c).

$\nu_{a(COO-)}$ shifts to higher wavenumbers, thus indicating the inner-sphere nature of the formed complex [68].

It is worthwhile remarking here that the last three points of the adsorption isotherm shown in Fig. 7 correspond to three different SBA–MSA samples, which were synthesized in a totally separate manner; i.e., the preparation of the SBA-15 powder, of the TMSMSA precursor, and the post-functionalization of the scaffold were independently repeated. All of these points fall within ±2 mg g^{-1}, deviation that it is much less than the experimental uncertainty of the measured q_e values. This fact highlights the outstanding degree of reproducibility of our synthetic approach.

4. Conclusions

This work demonstrates an easy approach for immobilizing free, readily available, COOH groups on the surface of mesoporous SBA-15. It can foreseeable be extended to other mesoporous silica materials as well to other oxide surfaces. The derivatization of

silane with carboxylic acids through the photochemically induced thiol-ene reaction requires a simple experimental setup, has conversions better than 99%, and does not require tedious purification procedures. Moreover, this method can take advantage of the vast library of thiol based compounds aimed to Au surfaces functionalization [69].

This simple synthetic scheme adds to chemical "toolbox" for mesoporous materials functionalization and opens an exciting venue for SiO_2 and transition metal oxide surface modification where precise control of the immobilized molecules is required.

Acknowledgments

M.V.L. acknowledges a postdoctoral fellowship from CONICET. A.V.B., A.E.R., G.J.A.A.S.I. and A.W. are permanent research fellows of CONICET. We thank Dr. C. Spagnuolo for assistance on NMR measurements, Dr. Victor Luca (CNEA) for assistance N_2 sorption measurements, Dr. Matheus Cardoso for invaluable help on LNLS beamline SAXS1 (Projects SAXS1 – 13608) and Dr. Andrés Zelcer for assistance on SAXS measurements. This work was funded in part by ANPCyT (PICT 2012-2087, PICT 2013-1303).

Appendix A. Supplementary material

Supplementary data associated with this article can be found, in the online version, at http://dx.doi.org/10.1016/j.jcis.2015.03.030.

References

[1] Z. Wu, D. Zhao, Chem. Commun. 47 (2011) 3332–3338.
[2] D. Zhao, Y. Wan, W. Zhou, Ordered Mesoporous Materials, John Wiley & Sons, 2012.
[3] M. Vallet-Regí, F. Balas, D. Arcos, Angew. Chem. – Int. Ed. 46 (2007) 7548–7558.
[4] P. Yang, S. Gai, J. Lin, Chem. Soc. Rev. 41 (2012) 3679–3698.
[5] A. Brunsen, J. Cui, M. Ceolín, A.D. Campo, G.J.A.A. Soler-Illia, O. Azzaroni, Chem. Commun. 48 (2012) 1422–1424.
[6] A. Brunsen, C. Díaz, L.I. Pietrasanta, B. Yameen, M. Ceolín, G.J.A.A. Soler-Illia, O. Azzaroni, Langmuir 28 (2012) 3583–3592.
[7] K. Patel, S. Angelos, W.R. Dichtel, A. Coskun, Y.W. Yang, J.I. Zink, J.F. Stoddart, J. Am. Chem. Soc. 130 (2008) 2382–2383.
[8] A. Bhaumik, T. Tatsumi, J. Catal. 189 (2000) 31.
[9] T. Kang, Y. Park, J. Yi, Ind. Eng. Chem. Res. 43 (2004) 1478–1484.
[10] V. López-Puente, S. Abalde-Cela, P.C. Angelomé, R.A. Alvarez-Puebla, L.M. Liz-Marzán, J. Phys. Chem. Lett. 4 (2013) 2715–2720.
[11] A. Katiyar, L. Ji, P. Smirniotis, N.G. Pinto, J. Chromatogr. A 1069 (2005) 119–126.
[12] D. Van Gough, A. Wolosiuk, P.V. Braun, Nano Lett. 9 (2009) 1994–1998.
[13] L. Ma, D.J. Mihalcik, W. Lin, J. Am. Chem. Soc. 131 (2009) 4610–4612.
[14] T. Mallat, A. Baiker, Chem. Rev. 104 (2004) 3037–3058.
[15] H.T. Shiu, B. Goss, C. Lutton, R. Crawford, Y. Xiao, J. Mater. Chem. B 2 (2014) 3009–3021.
[16] M.A. Blesa, P.J. Morando, A.E. Regazzoni, Chemical Dissolution of Metal Oxides, CRC Press, Boca Raton, 1994.
[17] C.L. Lin, C.F. Lee, W.Y. Chiu, J. Colloid Interface Sci. 291 (2005) 411–420.
[18] S.S. Wong, Chemistry of Protein Conjugation and Cross-linking, CRC press, 1991.
[19] M.A. Markowitz, P.E. Schoen, P. Kust, B.P. Gaber, Colloids Surf. A: Physicochem. Eng. Aspects 150 (1999) 85–94.
[20] D. Son, A. Wolosiuk, P.V. Braun, Chem. Mater. 21 (2009) 628–634.
[21] L. Han, Y. Sakamoto, O. Terasaki, Y. Li, S. Che, J. Mater. Chem. 17 (2007) 1216–1221.
[22] J. Gu, J. Liu, Y. Li, W. Zhao, J. Shi, Langmuir 29 (2013) 403–410.
[23] M. Colilla, I. Izquierdo-Barba, S. Sánchez-Salcedo, J.L.G. Fierro, J.L. Hueso, M. Vallet-Regí, Chem. Mater. 22 (2010) 6459–6466.
[24] L. Han, O. Terasaki, S. Che, J. Mater. Chem. 21 (2011) 11033–11039.
[25] N. Liu, R.A. Assink, C.J. Brinker, Chem. Commun. 9 (2003) 370–371.
[26] C.M. Yang, B. Zibrowius, F. Schüth, Chem. Commun. 9 (2003) 1772–1773.
[27] Z. Yan, S. Tao, J. Yin, G. Li, J. Mater. Chem. 16 (2006) 2347–2353.
[28] Q. Yang, S. Wang, P. Fan, L. Wang, Y. Di, K. Lin, F.S. Xiao, Chem. Mater. 17 (2005) 5999–6003.
[29] A. El Kadib, N. Katir, A. Finiels, A. Castel, N. Marcotte, K. Molvinger, C. Biolley, P. Gaveau, M. Bousmina, D. Brunel, Dalton Trans. 42 (2013) 1591–1602.
[30] C.D. Bain, G.M. Whitesides, Langmuir 5 (1989) 1370–1378.
[31] C.E. Hoyle, C.N. Bowman, Angew. Chem. – Int. Ed. 49 (2010) 1540–1573.
[32] X. Cattoën, A. Noureddine, J. Croissant, N. Moitra, K. Bürglová, J. Hodačová, O. De Los, J. Sol Gel Sci. Technol. 70 (2014) 245–253.
[33] N. Moitra, J.J.E. Moreau, X. Cattoën, M. Wong, Chem. Commun. 46 (2010) 8416–8418.
[34] H.C. Kolb, M.G. Finn, K.B. Sharpless, Angew. Chem. – Int. Ed. 40 (2001) 2004–2021.
[35] M.A. White, J.A. Johnson, J.T. Koberstein, N.J. Turro, J. Am. Chem. Soc. 128 (2006) 11356–11357.
[36] N.B. Cramer, J.P. Scott, C.N. Bowman, Macromolecules 35 (2002) 5361–5365.
[37] C.R. Morgan, F. Magnotta, A.D. Ketley, J. Polym. Sci.: Polym. Chem. Ed. 15 (1977) 627–645.
[38] A. Gress, A. Völkel, H. Schlaad, Macromolecules 40 (2007) 7928–7933.
[39] C.-H. Wong, S.C. Zimmerman, Chem. Commun. 49 (2013) 1679–1695.
[40] C.E. Hoyle, A.B. Lowe, C.N. Bowman, Chem. Soc. Rev. 39 (2010) 1355–1387.
[41] A.K. Tucker-Schwartz, R.A. Farrell, R.L. Garrell, J. Am. Chem. Soc. 133 (2011) 11026–11029.
[42] D. Zhao, Q. Huo, J. Feng, B.F. Chmelka, G.D. Stucky, J. Am. Chem. Soc. 120 (1998) 6024–6036.
[43] T. Callan, J.A.R. Henderson, Analyst 54 (1929) 650–653.
[44] SDBSWeb: http://sdbs.db.aist.go.jp (National Institute of Advanced Industrial Science and Technology), SDBS No. 23246.
[45] S. Patai, Z. Rappoport, Y. Apeloig, The Chemistry of Organic Silicon Compounds, Wiley, 1989.
[46] D. Brühwiler, Nanoscale 2 (2010) 887–892.
[47] M.V. Lombardo, M. Videla, A. Calvo, F.G. Requejo, G.J.A.A. Soler-Illia, J. Hazard. Mater. 223–224 (2012) 53–62.
[48] A. Davidson, Curr. Opin. Colloid Interface Sci. 7 (2002) 92–106.
[49] S. Pikus, L.A. Solovyov, M. Kozak, M. Jaroniec, Appl. Surf. Sci. 253 (2007) 5682–5687.
[50] L.A. Solovyov, Chem. Soc. Rev. 42 (2013) 3708–3720.
[51] M. Thommes, Chem. Ing. Tech. 82 (2010) 1059–1073.
[52] S. Lowell, J. Shields, M. Thomas, M. Thommes, Mesopore Analysis, Characterization of Porous Solids and Powders: Surface Area, Pore Size and Density, Springer, Netherlands, 2004, pp. 101–128.
[53] F. Rouquerol, J. Rouquerol, K. Sing, Chapter 7 – assessment of mesoporosity, in: F. Rouquerol, J. Rouquerol, K. Sing (Eds.), Adsorption by Powders and Porous Solids, Academic Press, London, 1999, pp. 191–217.
[54] N. Hüsing, U. Schubert, Porous inorganic–organic hybrid materials, Functional Hybrid Materials, Wiley-VCH Verlag GmbH & Co. KGaA, 2005.
[55] R.J. Dombrowski, D.R. Hyduke, C.M. Lastoskie, Langmuir 16 (2000) 5041–5050.
[56] L.T. Zhuravlev, Colloids Surf. A: Physicochem. Eng. Aspects 173 (2000) 1–38.
[57] O. Gershevitz, C.N. Sukenik, J. Am. Chem. Soc. 126 (2004) 482–483.
[58] S. Fiorilli, B. Camarota, E. Garrone, B. Onida, Phys. Chem. Chem. Phys. 13 (2011) 1201–1209.
[59] S. Fiorilli, B. Onida, B. Bonelli, E. Garrone, J. Phys. Chem. B 109 (2005) 16725–16729.
[60] S.S. Cheng, D.A. Scherson, C.N. Sukenik, Langmuir 11 (1995) 1190–1195.
[61] B. González, M. Colilla, C.L. De Laorden, M. Vallet-Regí, J. Mater. Chem. 19 (2009) 9012–9024.
[62] G.R. Lenz, A.E. Martell, Inorg. Chem. 4 (1965) 378–384.
[63] J.T. Edsall, J. Wyman, Biophysical chemistry, Thermodynamics, Electrostatics, and the Biological Significance of the Properties of Matter, vol. 1, Academic Press, 1958.
[64] M. Ajmal, A. Hussain, Water Res. 32 (1998) 3085–3091.
[65] D.G. Strawn, L.L. Baker, Environ. Sci. Technol. 42 (2008) 37–42.
[66] H.P. Gregor, L.B. Luttinger, E.M. Loebl, J. Phys. Chem. 59 (1955) 34–39.
[67] A. Walcarius, M. Etienne, B. Lebeau, Chem. Mater. 15 (2003) 2161–2173.
[68] K. Nakamoto, Infrared and Raman Spectra of Inorganic and Coordination Compounds, Applications in Coordination, Organometallic, and Bioinorganic Chemistry, John Wiley & Sons, 2009.
[69] A.C. Templeton, W.P. Wuelfing, R.W. Murray, Acc. Chem. Res. 33 (2000) 27–36.